

Simulations of polarimetric observations of debris disks through the Roman Coronagraph Instrument

Ramya M Anche^a, Ewan S. Douglas^a, Kian Milani^{a,b}, Jaren Ashcraft^{a,b}, and John Debes^c

^aSteward Observatory, University of Arizona, 933N Cherry Avenue, Tucson, Arizona, 85721, USA

^bJames C. Wyant College of Optical Sciences, University of Arizona, 933N Cherry Avenue, Tucson, Arizona, 85721, USA

^cSpace Telescope Science Institute, 3700 San Martin Drive, Baltimore, MD 21218, USA

ABSTRACT

The Roman coronagraph instrument will demonstrate high-contrast imaging technology, enabling the imaging of faint debris disks, the discovery of inner dust belts, and planets. Polarization studies of debris disks provide information on dust grains' size, shape, and distribution. The Roman coronagraph uses a polarization module comprising two Wollaston prism assemblies to produce four orthogonally polarized images (I_0 , I_{90} , I_{45} , and I_{135}), each measuring 3.2 arcsecs in diameter and separated by 7.5 arcsecs in the sky. The expected RMS error in the linear polarization fraction measurement is 1.66% per resolution element of 3 by 3 pixels. We present a mathematical model to simulate the polarized intensity images through the Roman CGI, including the instrumental polarization and other uncertainties. We use disk modeling software, MCFOST, to model q , u , and polarization intensity of the debris disk, Epsilon-Eridani. The polarization intensities are convolved with the coronagraph throughput incorporating the PSF morphology. We include model uncertainties, detector noise, speckle noise, and jitter. The final polarization fraction of 0.4 ± 0.0251 is obtained after the post-processing.

Keywords: Roman CGI, Debris disks, Polarization observations, coronagraphs, Polarimetric calibration

1. INTRODUCTION

Debris disks are predominantly made of dust and planetesimals and are found to be an integral part of the evolution of the planetary systems.^{1,2} The Asteroid belt and the Kuiper belt form the debris disk of our solar system along with the zodiacal dust.³ Debris disks may be polarized due to Rayleigh/Mie scattering by dust particles or asymmetry or the dichroic extinction of the dust grains in the presence of magnetic fields. Polarization observations of debris disks enable us to constrain their structure and properties of the dust grains such as composition, size, shape, and distribution.⁴⁻⁷ Polarization observation of several debris disks has been carried out using the Gemini Planet Imager (GPI)⁸ at the Gemini Telescope, and SPHERE-ZIMPOL⁹ at the Very Large Telescope (VLT) in the near IR wavelengths. Hubble Space Telescope Advanced Camera for Surveys coronagraph has been used to observe the polarization of a few debris disks (HD61005,¹⁰ and AU Mic¹¹) in the Johnson-Cousins V band filter. The multi-band polarization observations will allow us to constrain better the dust properties and disk structure of the debris disks.

The upcoming Nancy Grace Roman Space Telescope Coronagraph instrument (CGI) will facilitate the polarization observations of fainter debris disks (reaching contrast level of $\sim 10^{-8}$) around the nearby stars in addition to the high-contrast and high-resolution imaging of exoplanets. The polarimetric module consists of two Wollaston prisms, each producing two orthogonally polarized images, separated by 7.5" on the sky. The imaging polarimetry is available for the narrow field (525nm), and wide-field (825nm) modes.¹² In this paper, we describe a mathematical model for simulating the polarization observations of debris disk through the Roman CGI. In our simulations, we have considered the debris disk around a nearby (early) sun-like star, Epsilon Eridani (ϵ Eridani).

The next section provides an overview of the mathematical model and a snapshot of each stage's results. The following sections describe each step in the mathematical model with the corresponding outputs. Finally, the conclusions and future work are presented in the discussion section.

Further author information: (Send correspondence to R.M.A)
R.M.A: E-mail: ramyaanche@arizona.edu

2. MATHEMATICAL MODEL

In this section, we describe the overview of the mathematical model developed for the simulation of polarization observation of debris disk Epsilon-Eridani as shown in Figure 1. First, the disk is modeled using **MCFOST** to obtain the scattered light intensity and Stokes parameters. Next, the disk intensities are convolved with the Roman CGI PSF obtained using the **PROPER** models. Further, the EMCCD photon counted images are generated, including the EMCCD gain and noise characteristics. Next, we add the speckle and jitter noise using **Os9** simulations of Roman CGI and perform disk extraction. The final step is the estimation of Stokes parameters and corresponding errors after multiplying the instrument Mueller matrix. Each stage of this model is described in the following sections.

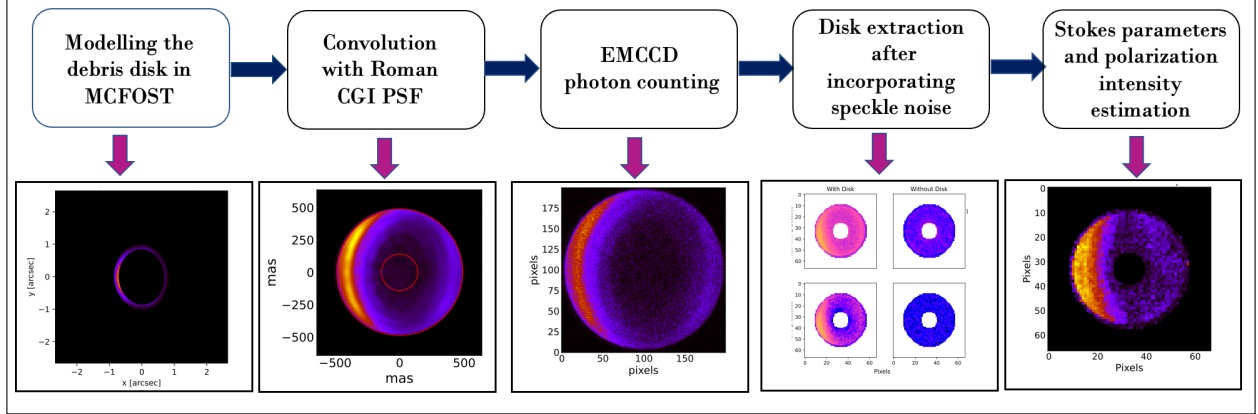


Figure 1. Mathematical model for simulating the polarization of debris disk through Roman CGI

3. MODELLING OF EPSILON-ERIDANI IN MCFOST

Epsilon Eridani is a star similar to the early sun; at a distance of 3.2pc with $T=5100\text{K}$, $\text{Mass}=0.82M_{\odot}$ and $\text{Radius}=0.88R_{\odot}$. The debris disk around ϵ Eridani has been observed at multiple wavelengths, yet, the disk parameters and details of the structure are debatable. The debris disk has been detected as an unresolved excess around the star with two or three components: a warm inner disk with \sim two narrow belts according to *Su et. al(2017)*¹³ (that has not yet been resolved) and a cold outer disk imaged with both ALMA¹⁴ and other Sub-millimeter instruments.^{15,16}

The Roman CGI is expected to resolve the innermost disk around ϵ Eridani and provide clarity regarding the size and location of the inner disk. We have used the disk parameters and dust composition from *Su et.al(2017)*¹³ to model the inner disk of the ϵ Eridani. The parameters provided in Table 1 are used in **MCFOST** to obtain the scattered light and Stokes parameters (for linear polarization: q , and u) images at a wavelength of 575nm and inclination of 34° . We used a 20.8 mas/pixel scale with 256×256 pixels and the Mie scattering model to account for the polarization. The scattered light images and Stokes parameters are shown in Figures 2 and 3 respectively.

The scattered light brightness and p and θ are used to obtain the four intensities (I_0 , I_{90} , I_{45} and I_{135}) as below:

$$I_0 = Nsrct * (1 + p * \cos(2 * \theta))/2 \quad I_{90} = Nsrct * (1 - p * \cos(2 * \theta))/2 \quad (1)$$

$$I_{45} = Nsrct * (1 + p * \sin(2 * \theta))/2 \quad I_{135} = Nsrct * (1 - p * \sin(2 * \theta))/2 \quad (2)$$

where $Nsrct$ correspond to the total number of photons. The four intensities are shown in Figure 4. These intensities are then convolved with the Roman CGI PSFs as explained in the next section.

Parameters	Eps-eri model	
Disks	2 disk	
Disk extent (AU)	1.5-2	8-20*
Scale Height	0	0
Dust Mass (Mo)	$1.35 \cdot 10^{-12}$	$1.00 \cdot 10^{-12}$
Surface density Exponent	-10 to -10	-10 to -10
Grain sizes(microns)	1-1000 $e^{3.65}$	1-1000 $e^{3.65}$
Grain composition	Astrosilicates	Ice-silicates

Table 1. Parameters used in the MCFOST modelling of ϵ Eridani. * is not visible in figure 2

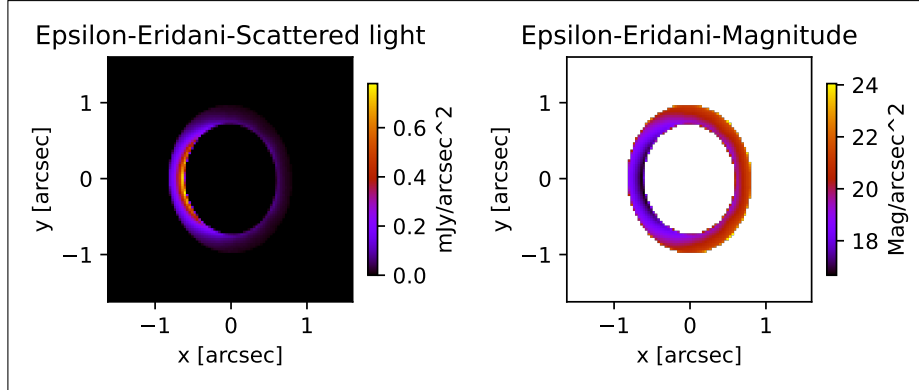


Figure 2. Scattered light brightness and magnitude obtained (for the innermost disk) using [MCFOST](#) at $\lambda=575\text{nm}$

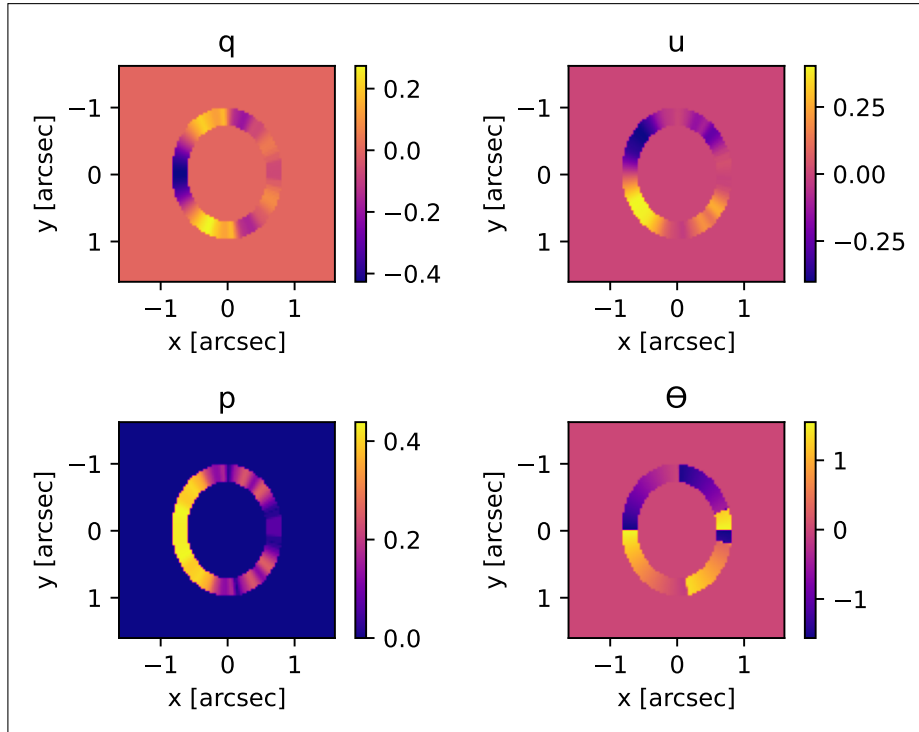


Figure 3. Stokes parameters obtained (for the innermost disk) using [MCFOST](#) at $\lambda=575\text{nm}$

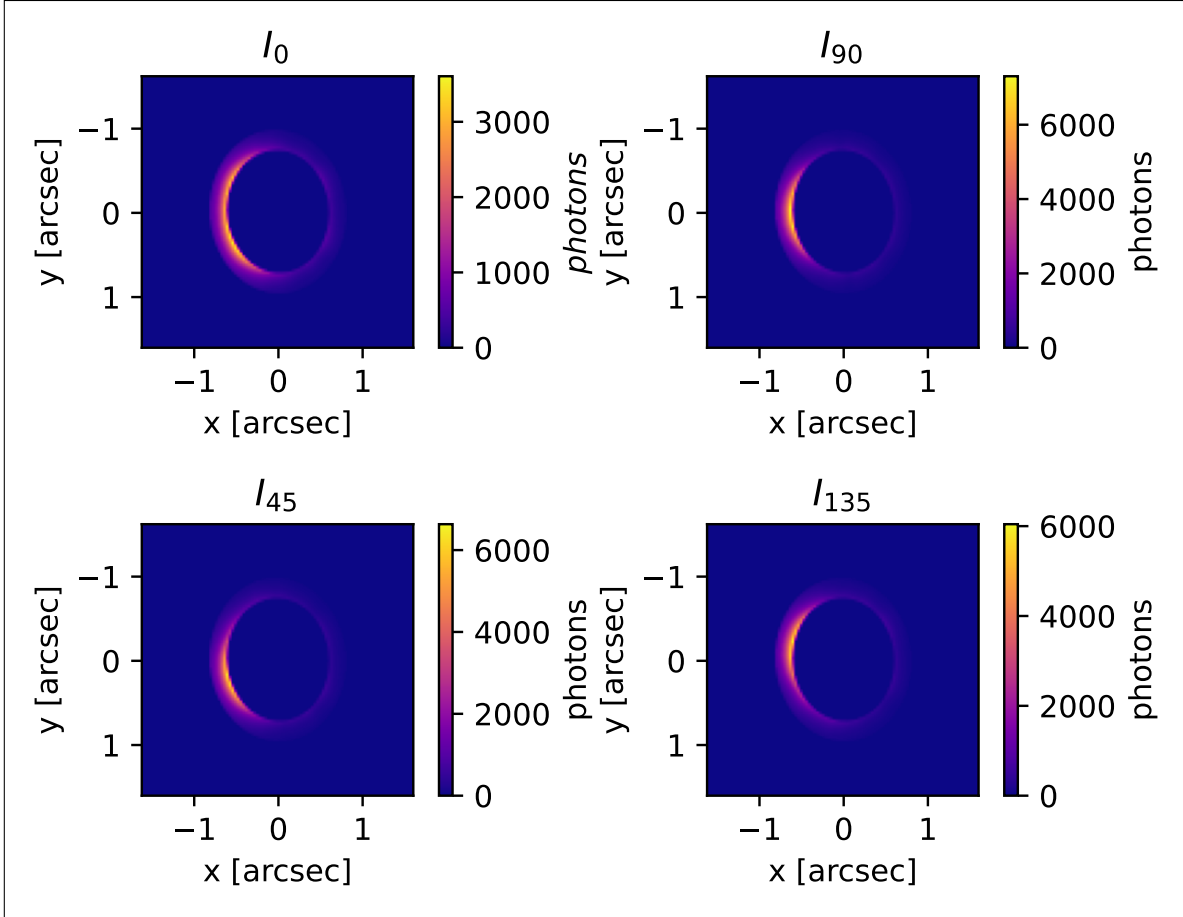


Figure 4. Polarization intensities estimated using p , θ and Scattered light brightness at $\lambda=575\text{nm}$

4. GENERATING ROMAN PSFS

Point Response Functions (PRFs) are generated for the Hybrid Lyot Coronagraph mode at 575nm with a field of view of $0.14''\text{-}0.45''$ using [PROPER](#) model of the Roman CGI. We set the polarization axis as the mean of all polarization modes in the [PROPER](#) model (polaxis=10). Convolution is done via a matrix-vector multiplication in a process utilizing the PRFs of field angles for each pixel in the disk model array.¹⁷

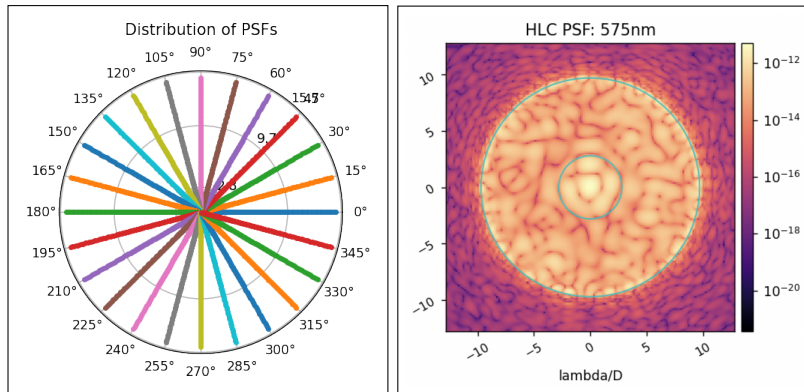


Figure 5. Distribution of PRFs used to create image simulations (left). On-axis monochromatic PSF for the HLC (right).

In addition, PRFs for field angles in both image dimensions are utilized to account for the roll angle. This is illustrated in Figure 5 with the distribution of PRFs used for the HLC. Finally, PRFs beyond the OWA are included to incorporate the scattering of light from regions of the disk outside the OWA. The disk images of I_0 , I_{90} , I_{45} , and I_{135} are shown in Figure 6 after convolving with the Roman PSFs.

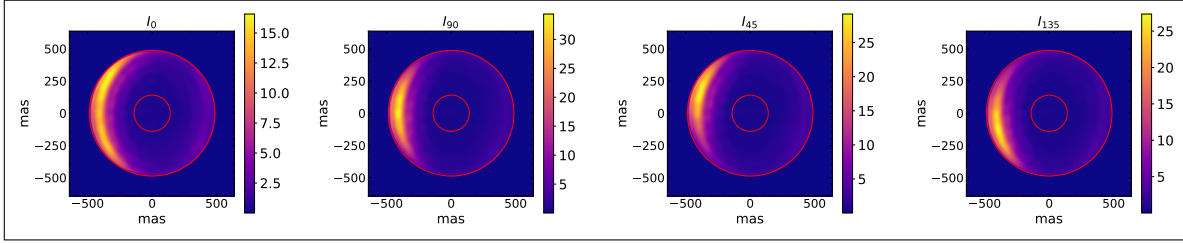


Figure 6. Polarization intensities (photons) after convolving with the PSF

5. EMCCD SIMULATION

The Roman CGI will use [e2v CCD201-20](#) which is a back-illuminated electron-multiplying CCD sensor consisting of 1024×1024 pixels of $13\mu\text{m}$ in size. It can be operated in low gain (<1000) and high gain (>1000) mode. To convert the disk polarization intensities to photo electrons [EMCCD detect](#)¹⁸ is used. We simulate a stack of 50 EMCCD frames for each of the intensity component with an exposure time=5s/frame, gain=800 incorporating bias= $10000e^-$, dark current = $0.0028, e^-/pix/s$, read noise= $100 e^-$. Figure 7 shows one of the frames at the EMCCD for all the four polarization intensities.

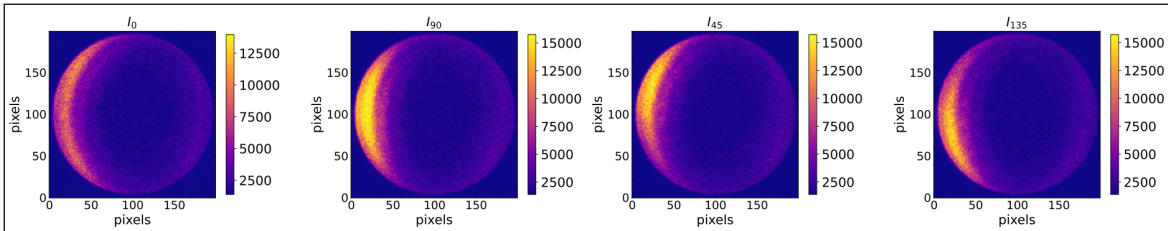


Figure 7. Polarization intensities for one of the EMCCD frames from the stack

6. DISK EXTRACTION AND ESTIMATING STOKES PARAMETERS

The integrated modeling team at JPL creates Observing Scenario simulations to generate the simulated science data for the HLC and SPC coronagraphs using the most recent version of the observation strategy. [OS9](#) is the ninth public release of Roman post-coronagraph simulated science images, which includes end-to-end Structural Thermal Optical Performance (STOP) model of the Roman observatory, coronagraph masks, diffraction, wavefront control, and detector noise and also jitter. We perform the disk processing, and extraction technique as explained in [Douglas et. al\(2022\)](#).¹⁹ The photon-counting procedure is operated on all the intensity images with a threshold of $1.1 \times \text{readnoise}$, following the steps from [Nemati\(2020\)](#).¹⁸ We include optical model uncertainty factors (MUFs) in our analysis obtained from the OS9 repository. Although we use the Non-negative matrix factorization (NMF) method²⁰ to subtract the PSF components while performing disk extraction, we can obtain the required SNR without using the NMF as well. Figure 8 shows the unprocessed coronagraphic images with and without disk and post-processed disk with NMF speckle subtraction for one of the polarization intensity components. Once the photon counted images are obtained for all the four intensity components, the Stokes parameters and corresponding errors are estimated as follows:²¹

$$q' = \frac{I_{0^\circ} - I_{90^\circ}}{I_{0^\circ} + I_{90^\circ}} \quad u' = \frac{I_{45^\circ} - I_{135^\circ}}{I_{45^\circ} + I_{135^\circ}} \quad (3)$$

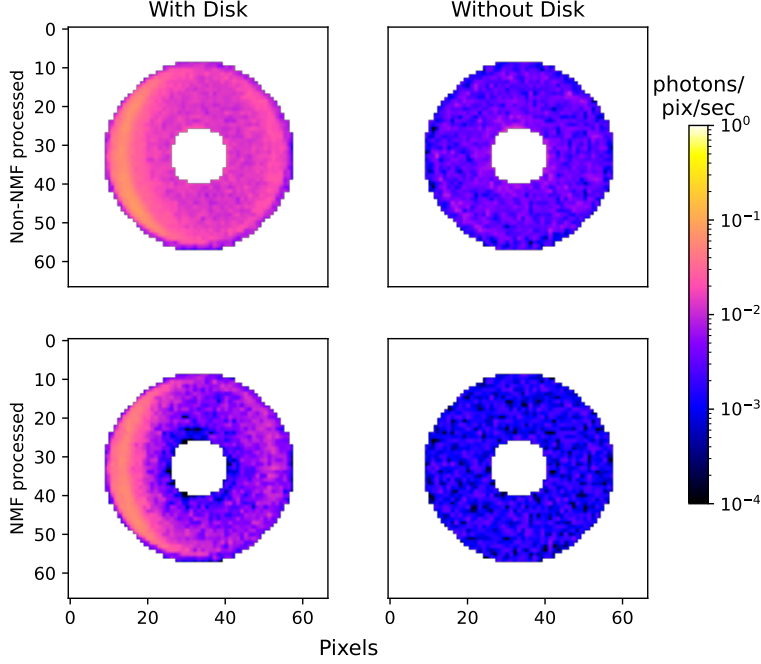


Figure 8. Top: raw, unprocessed coronagraphic images with and without disk injection, Bottom: NMF speckle subtraction post-processing applied - for I_0 component

$$\sigma_q = \sqrt{\frac{4 \left(I_{90^\circ}^2 \sigma_{I_0^\circ}^2 + I_0^\circ \sigma_{I_{90^\circ}}^2 \right)}{(I_0^\circ + I_{90^\circ})^4}}, \quad \sigma_u = \sqrt{\frac{4 \left(I_{45^\circ}^2 \sigma_{I_{135^\circ}}^2 + I_{135^\circ}^2 \sigma_{I_{45^\circ}}^2 \right)}{(I_{45^\circ} + I_{135^\circ})^4}} \quad (4)$$

where, $I_0^\circ, I_{90^\circ}, I_{45^\circ}, I_{135^\circ}$ are the four intensities in polarized beams and $\sigma_{I_0^\circ}, \sigma_{I_{90^\circ}}, \sigma_{I_{45^\circ}}, \sigma_{I_{135^\circ}}$ are corresponding uncertainties. Although all the instrument effects are considered in the PSF convolution and OS9 simulations, we have not incorporated the polarization changes introduced by the Roman telescope and instrument optics. Any optical component in the system can either introduce or modify the incoming source polarization causing instrumental polarization, or polarization crosstalk.^{22,23} These effects can be accounted for using the 4×4 Mueller matrix of the system, as explained in the next section.

7. MUELLER MATRIX OF THE CGI INSTRUMENT AND ESTIMATING FINAL STOKES PARAMETERS

The pupil averaged Mueller matrices obtained from IPAC for wavelength 450-950nm is shown in Figure 9. We use the Mueller matrix for 575nm to obtain the final Stokes parameters as shown:

$$\begin{pmatrix} 1 \\ q \\ u \\ v \end{pmatrix} = \begin{pmatrix} M_{11} & M_{12} & M_{13} & M_{14} \\ M_{21} & M_{22} & M_{23} & M_{24} \\ M_{31} & M_{32} & M_{33} & M_{34} \\ M_{41} & M_{42} & M_{43} & M_{44} \end{pmatrix} \begin{pmatrix} 1 \\ q' \\ u' \\ 0 \end{pmatrix}. \quad (5)$$

where q' and u' are the stokes parameters obtained after the disk extraction. For measurement of linear polarization ($v'=0$), we consider the 3×3 Mueller matrix terms and estimate q, u as:

$$q = M_{21} + M_{22} * q' + M_{23} * u' \quad (6)$$

$$u = M_{31} + M_{32} * q' + M_{33} * u' \quad (7)$$

The p and θ are calculated as,

$$p = \sqrt{q^2 + u^2} \quad \theta = 0.5 \arctan \frac{u}{q}. \quad (8)$$

$$\sigma_p = \frac{\sqrt{(q^2\sigma_q^2 + u^2\sigma_u^2)}}{q^2 + u^2} \quad \sigma_\theta = 0.5p \frac{\sqrt{(u^2\sigma_q^2 + q^2\sigma_u^2)}}{q^2 + u^2} \quad (9)$$

Figures 10 and 11 show the final Stokes parameters and polarization fraction along with their errors. We compare the Stokes parameters obtained from MCFOST (Figure 3) for ϵ -Eridani to the final estimated Stokes parameters. The sign of q is found to be flipped due to the Mueller matrix element M_{21} . We recover all the Stokes parameters and the polarization fraction after incorporating various error factors in the Roman CGI.

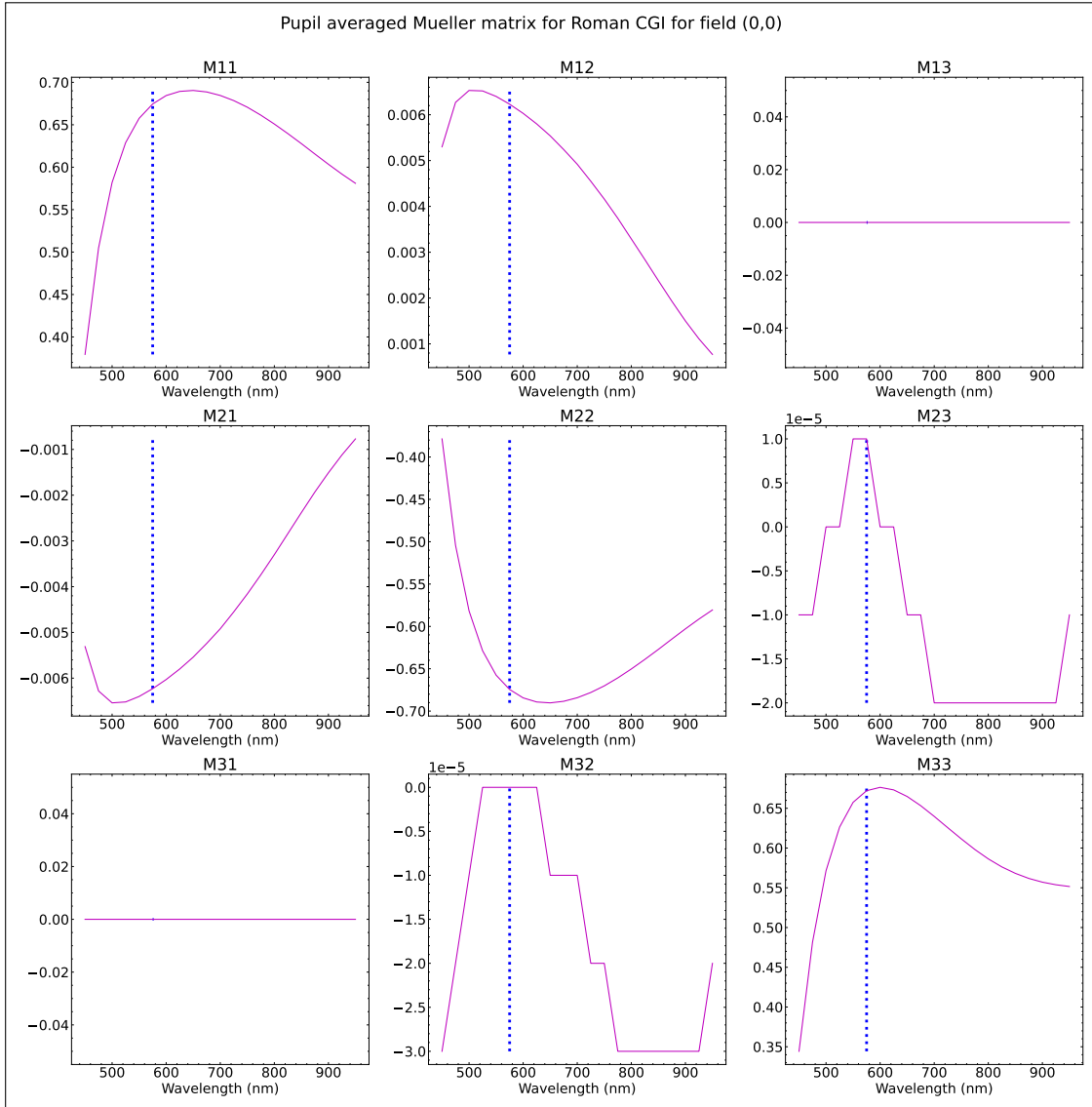


Figure 9. Pupil averaged Mueller matrix for Roman CGI for on-axis field obtained from IPAC. The dotted blue line shows the values of the matrix elements used in this analysis at $\lambda=575$ nm

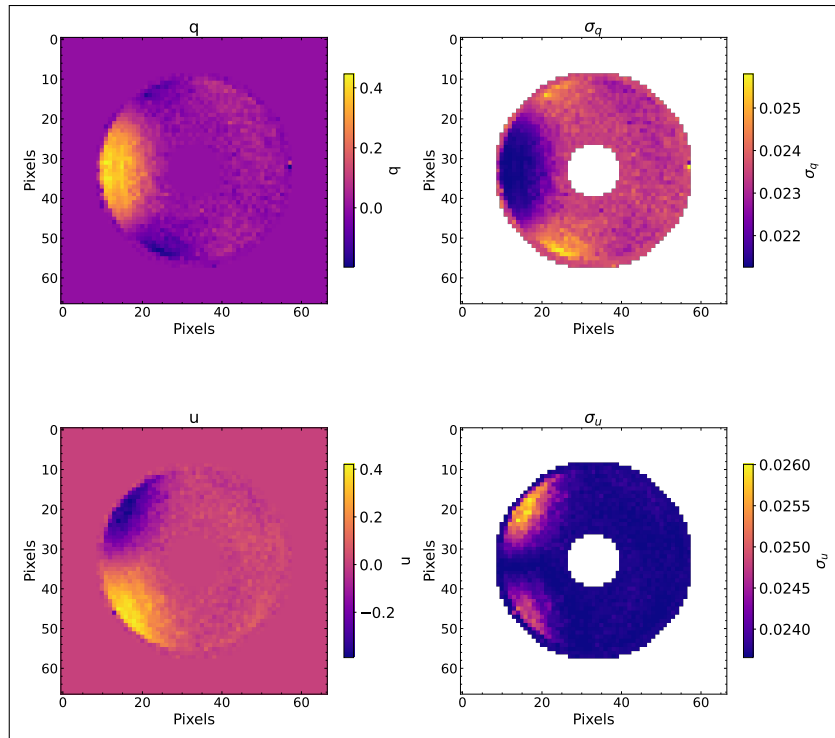


Figure 10. Stokes q and u and their corresponding errors estimated from the extracted disks

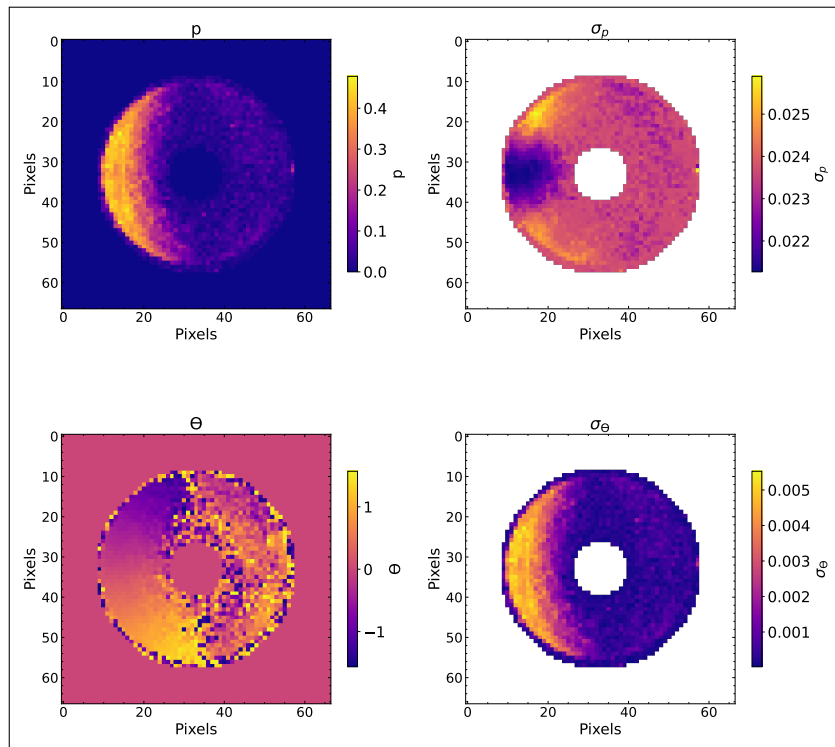


Figure 11. Stokes p and θ and their corresponding errors estimated from the extracted disks

8. DISCUSSION AND FUTURE WORK

We have presented a mathematical model to simulate polarization simulation of any debris disk through the Roman CGI. As an example, we have modeled the inner ring of the debris disk around Epsilon-Eridani. Various instrument errors, noise, and polarization effects have been accounted for, and we have recovered the input polarization fraction of 0.4 ± 0.025 . The error (2.5% per pixel) in the polarization fraction measurement is comparable to the expected RMS error for the Roman CGI. Also, this accuracy may suffice for the polarimetry of disks in general, as the linear polarization fraction of disks is in the order of percent to several tens of percent compared to the other stellar objects. However, the achievable measurement accuracy depends on how well the instrument can be calibrated to correct for various polarimetric errors introduced by the instrument optics. Hence a detailed polarization calibration strategy is required for planning the observations of polarized and unpolarized standard stars and performing the required polarization corrections using those observations.^{24,25}

The MCFOST model for Epsilon-Eridani is simulated using a single grain composition. We would model the disk by varying dust grain sizes, shapes, and compositions and obtain the wavelength dependence of scattering polarization.²⁶ This analysis will enable us to understand how well the disk properties can be constrained using multi-band polarization measurements.

ACKNOWLEDGMENTS

Portions of this work were supported by the WFIRST Science Investigation team prime award #NNG16PJ24 and the Arizona Board of Regents Technology Research Initiative Fund (TRIF). The authors would like to thank Dr. Max Miller-Blanchaer (UCSB) for the useful discussions and Dr. Bertrand Mennesson (JPL) for generating the Mueller matrices.

REFERENCES

- [1] Hughes, A. M., Duchêne, G., and Matthews, B., “Debris disks: Structure, composition, and variability,” *arXiv preprint arXiv:1802.04313* (2018).
- [2] Backman, D., “Debris disks: An overview,” *Debris Disks and the Formation of Planets* **324**, 9 (2004).
- [3] Wyatt, M. C. and Jackson, A. P., “Insights into planet formation from debris disks,” *Space Science Reviews* **205**(1), 231–265 (2016).
- [4] Crotts, K. A., Matthews, B. C., Esposito, T. M., Duchêne, G., Kalas, P., Chen, C. H., Arriaga, P., Millar-Blanchaer, M. A., Debes, J. H., Draper, Z. H., et al., “A deep polarimetric study of the asymmetrical debris disk hd 106906,” *The Astrophysical Journal* **915**(1), 58 (2021).
- [5] Hull, C. L., Yang, H., Cortés, P. C., Dent, W. R., Kral, Q., Li, Z.-Y., Le Gouellec, V. J., Hughes, A. M., Milli, J., Teague, R., et al., “Polarization from aligned dust grains in the β pic debris disk,” *The Astrophysical Journal* **930**(1), 49 (2022).
- [6] Chen, C., Mazoyer, J., Poteet, C. A., Ren, B., Duchêne, G., Hom, J., Arriaga, P., Millar-Blanchaer, M. A., Arnold, J., Bailey, V. P., et al., “Multiband gpi imaging of the hr 4796a debris disk,” *The Astrophysical Journal* **898**(1), 55 (2020).
- [7] Engler, N., Schmid, H. M., Thalmann, C., Boccaletti, A., Bazzon, A., Baruffolo, A., Beuzit, J.-L., Claudi, R., Costille, A., Desidera, S., et al., “The hip 79977 debris disk in polarized light,” *Astronomy & Astrophysics* **607**, A90 (2017).
- [8] Macintosh, B., Graham, J. R., Ingraham, P., Konopacky, Q., Marois, C., Perrin, M., Poyneer, L., Bauman, B., Barman, T., Burrows, A. S., et al., “First light of the gemini planet imager,” *proceedings of the National Academy of Sciences* **111**(35), 12661–12666 (2014).
- [9] Beuzit, J.-L., Feldt, M., Dohlen, K., Mouillet, D., Puget, P., Antichi, J., Baruffolo, A., Baudoz, P., Berton, A., Boccaletti, A., et al., “Sphere: A planet finder instrument for the vlt,” *The messenger* **125**, 29 (2006).
- [10] Maness, H., Kalas, P., Peek, K., Chiang, E., Scherer, K., Fitzgerald, M., Graham, J. R., Hines, D., Schneider, G., and Metchev, S., “Hubble space telescope optical imaging of the eroding debris disk hd 61005,” *The Astrophysical Journal* **707**(2), 1098 (2009).
- [11] Graham, J. R., Kalas, P. G., and Matthews, B. C., “The signature of primordial grain growth in the polarized light of the au microscopii debris disk,” *The Astrophysical Journal* **654**(1), 595 (2007).

- [12] Mennesson, B., Bailey, V., Zellem, R., Zimmerman, N., Ygouf, M., Hildebrandt, S. R., Rhodes, J., Kasdin, J., Macintosh, B., Turnbull, M., et al., “The roman space telescope coronagraph technology demonstration: current status and relevance to future missions,” in [*Techniques and Instrumentation for Detection of Exoplanets X*], **11823**, 1182310, International Society for Optics and Photonics (2021).
- [13] Su, K. Y., De Buizer, J. M., Rieke, G. H., Krivov, A. V., Lohne, T., Marengo, M., Stapelfeldt, K. R., Balering, N. P., and Vacca, W. D., “The inner 25 au debris distribution in the ϵ eri system,” *The Astronomical Journal* **153**(5), 226 (2017).
- [14] Booth, M., Dent, W. R., Jordán, A., Lestrade, J.-F., Hales, A. S., Wyatt, M. C., Casassus, S., Ertel, S., Greaves, J. S., Kennedy, G. M., et al., “The northern arc of ϵ eridani’s debris ring as seen by alma,” *Monthly Notices of the Royal Astronomical Society* **469**(3), 3200–3212 (2017).
- [15] Backman, D., Marengo, M., Stapelfeldt, K., Su, K., Wilner, D., Dowell, C., Watson, D., Stansberry, J., Rieke, G., Megeath, T., et al., “Epsilon eridani’s planetary debris disk: structure and dynamics based on spitzer and caltech submillimeter observatory observations,” *The Astrophysical Journal* **690**(2), 1522 (2008).
- [16] Greaves, J., Holland, W., Wyatt, M., Dent, W., Robson, E., Coulson, I., Jenness, T., Moriarty-Schieven, G., Davis, G., Butner, H., et al., “Structure in the ϵ eridani debris disk,” *The Astrophysical Journal* **619**(2), L187 (2005).
- [17] Milani, K. and Douglas, E. S., “Faster imaging simulation through complex systems: a coronagraphic example,” in [*Optical Modeling and Performance Predictions XI*], Kahan, M. A., ed., **11484**, 15 – 28, International Society for Optics and Photonics, SPIE (2020).
- [18] Nemati, B., “Photon counting and precision photometry for the roman space telescope coronagraph,” in [*Space Telescopes and Instrumentation 2020: Optical, Infrared, and Millimeter Wave*], **11443**, 884–895, SPIE (2020).
- [19] Douglas, E. S., Debes, J., Mennesson, B., Nemati, B., Ashcraft, J., Ren, B., Stapelfeldt, K. R., Savransky, D., Lewis, N. K., and Macintosh, B., “Sensitivity of the roman coronagraph instrument to exozodiacal dust,” *Publications of the Astronomical Society of the Pacific* **134**(1032), 024402 (2022).
- [20] Ren, B., Pueyo, L., Zhu, G. B., Debes, J., and Duchêne, G., “Non-negative matrix factorization: robust extraction of extended structures,” *The Astrophysical Journal* **852**(2), 104 (2018).
- [21] Ramaprakash, A., Rajarshi, C., Das, H., Khodade, P., Modi, D., Panopoulou, G., Maharana, S., Blinov, D., Angelakis, E., Casadio, C., et al., “Robopol: a four-channel optical imaging polarimeter,” *Monthly Notices of the Royal Astronomical Society* **485**(2), 2355–2366 (2019).
- [22] Tinbergen, J., “Astronomical polarimetry,” *Astronomical Polarimetry* (2005).
- [23] Anche, R. M., Sen, A. K., Anupama, G. C., Sankarasubramanian, K., and Skidmore, W., “Analysis of polarization introduced due to the telescope optics of the thirty meter telescope,” *Journal of Astronomical Telescopes, Instruments, and Systems* **4**(1), 018003 (2018).
- [24] Millar-Blanchaer, M. A., Perrin, M. D., Hung, L.-W., Fitzgerald, M. P., Wang, J. J., Chilcote, J., Graham, J. R., Bruzzone, S., and Kalas, P. G., “Gpi observational calibrations xiv: polarimetric contrasts and new data reduction techniques,” in [*Ground-based and Airborne Instrumentation for Astronomy VI*], **9908**, 993–1009, SPIE (2016).
- [25] van Holstein, R. G., Girard, J. H., De Boer, J., Snik, F., Milli, J., Stam, D., Ginski, C., Mouillet, D., Wahhaj, Z., Schmid, H. M., et al., “Polarimetric imaging mode of vlt/sphere/irdis-ii. characterization and correction of instrumental polarization effects,” *Astronomy & Astrophysics* **633**, A64 (2020).
- [26] Tazaki, R., Tanaka, H., Muto, T., Kataoka, A., and Okuzumi, S., “Effect of dust size and structure on scattered-light images of protoplanetary discs,” *Monthly Notices of the Royal Astronomical Society* **485**(4), 4951–4966 (2019).